Desalination and Water Treatment
www.deswater.com
doi: 10.5004/dwt.2020.26491

208 (2020) 377–385
December

Enhanced photocatalytic ozonation of 2,4-dichlorophenoxyacetic acid using P25/g-C_3N_4 composite under visible light irradiation

Yahong Zhou[a], Daiqiong Yang[a], Changyu Lu[a,b], Shuqi Dai[c], Jinlin Li[b], Weisheng Guan[b], Duo Li[a,*]

[a]*Hebei Province Key Laboratory of Sustained Utilization and Development of Water Resources, Hebei Province Collaborative Innovation Center for Sustainable Utilization of Water Resources and Optimization of Industrial Structure, School of Water Resources and Environment, Hebei GEO University, Shijiazhuang 050031, China, Tel. +86 311 87208372; emails: Liduo556688@126.com (D. Li), zhyh327@163.com (Y. Zhou), yangdaiqiong0510@126.com (D. Yang), pzpzlxl@163.com (C. Lu)*
[b]*Key Laboratory of Subsurface Hydrology and Ecological Effects in Arid Region, Ministry of Education, School of Water and Environment, Chang'an University, Xi'an 710064, Shaanxi, China, emails: cstsjz@163.com (J. Li), guanweisheng@263.net (W. Guan)*
[c]*South China Advanced Institute for Soft Matter Science and Technology, South China University of Technology, Guangzhou 510640, China, email: shuqidai@163.com (S. Dai)*

Received 20 April 2020; Accepted 20 August 2020

ABSTRACT

The heterojunction P25/g-C_3N_4 was successfully prepared by one-step method, and the phase structures, optical properties, morphology, charge separation, and transfer efficiency of obtained samples were characterized by X-ray diffraction, UV-visible, Fourier transform infrared, scanning electron microscopy, transmission electron microscopy, photoluminescence spectroscopy, respectively. The photocatalytic ozonation activity of samples was systematically evaluated by degrading 2.4-D under visible light irradiation. The results showed that P25/g-C_3N_4 heterojunction has remarkable catalytic activity and 3 wt.%-P25/g-C_3N_4 shows the best photocatalytic ozonation activity of 2,4-D (90.2%, 30 min, 30 mL/min O_3). The synergy factor between photocatalysis and ozonation is 9.34, indicating that increased synergy rate between photocatalysis and ozonation during the reaction. The cycling experiments show that catalyst 3 wt.%-P25/g-C_3N_4 has good stability and the trapping experiments indicate the main active substance in the reaction are $^{\bullet}O_3^-$ and $^{\bullet}OH$.

Keywords: P25/g-C_3N_4; Composite materials; Photocatalytic ozonation; 2,4-D

1. Introduction

In recent decades, herbicide pesticides have been widely used in modern agriculture. However, since the natural degradation rate of chemical pollutants is very slow, the accumulated residual herbicides has caused serious damage to the soil, water, and human health [1,2]. Semiconductor photocatalytic oxidation technology has been paid much attention to the treatment of chemical pollution due to their remarkable photocatalytic performance [3,4]. But photocatalytic activity of semiconductor photocatalytic catalyst was limited by its high recombination rate of photoinduced electrons, which seriously restricts its further practical application [5,6]. In order to resolve this problem, combining

* Corresponding author.

photocatalysis with other technologies has been arranged. Recently, photocatalytic ozonation, combining ozone oxidation, and photocatalytic oxidation is an ideal strategy for the treatment of the toxic and refractory organic pollutants [7]. The introduction of O_3 have strong scavenger effect, the surface electrons of semiconductor photocatalysts can be quickly trapped and used to produce $^{\bullet}O_3^-$, which could significantly promote the charge separation efficiency and further transform into hydroxyl radicals [8]. Therefore, there have more and more studies on the photocatalytic ozonation degradation of refractory organic pollutants and the combination of ozonation and photocatalysis is proved to be one of the most effective ways to enhance the performance of semiconductor photocatalytic catalyst [9,10]. For example, Li et al. [11] reported that $LaFeO_3$ nanoparticles can degrade 97% 2,4-D with the ozone concentration of 60 mL/min under visible light irradiation. It is mainly attributed to the synergistic effects between photocatalysis and ozonation owing to the powerful scavenger effect of ozone and strong activity of $^{\bullet}OH$. Sheydaei et al. [12] immobilize N–TiO_2 and GO on the surface of titan grid sheet and degraded cefixime under the visible light irradiation by the different process. The photocatalytic ozonation exhibit the highest degradation rate due to the synergism between N–TiO_2/GO photocatalyst and ozonation.

g-C_3N_4 is a kind of is a polymer semiconductor containing only two non-metal elements of carbon and nitrogen with narrower band gap (E_g = 2.7 eV) [13]. In 2009, Chen et al. [14] first reported the breakthrough of that semiconductor photocatalyst g-C_3N_4 catalyzed water to produce hydrogen and oxygen under visible light irradiation, thereafter g-C_3N_4 is considered to be a cheap, stable, and green photocatalyst due to low synthesis costs, environmental friendliness, simple operation, and high thermal and chemical stability [15,16]. In order to further improve the catalytic activity of g-C_3N_4, on the one hand researchers usually combined photolysis of g-C_3N_4 and ozonation, on the other hand they improved light absorption capacity and electron-hole separation efficiency of g-C_3N_4 by doping metal/nonmetal ion [17,18], loading precious metals [19], synthesis of composites [20,21], and formation of heterojunctions [22,23], etc. Theoretically, the construction of heterojunction composite photocatalyst is the simplest and effective method to suppress photo-generated carriers' recombination by steering the charge kinetics [24]. TiO_2 is one of the most promising semiconductor photocatalytic materials due to the advantages of high stability, nontoxicity, and low-cost [25]. When TiO_2 combined with g-C_3N_4, g-C_3N_4 could be easily excited under visible light, but it is hard for TiO_2. However, the photo-generated electrons on the conduction band(CB) of g-C_3N_4 would be transferred to the CB of TiO_2 and the photo-generated holes on the valence band (VB) of TiO_2 would be transferred to the VB of g-C_3N_4, which can effectively promote the transfer of photo-generated charges. To the best knowledge of the authors, some references on TiO_2/g-C_3N_4 binary catalyst have been already reported [26–28], but these investigations are mainly focusing on organic pollutant degradation [26], photocatalytic hydrogen production [27], and carbon dioxide reduction [28], the photocatalytic ozonation of 2,4-dichlorophenoxyacetic acid has not been reported, yet.

In this paper, a series of P25/g-C_3N_4 composite photocatalyst was prepared by one-step roasting method, and the photocatalytic performance of composites to degrade 2,4-D under visible light irradiation conditions was explored. The P25/g-C_3N_4 composite photocatalyst was combined with ozone to explore the synergistic effect of photocatalysis and ozonation, and the possible degradation mechanism were also discussed. We hope that the research in this article can provide a theoretical basis for the practical application of P25/g-C_3N_4 composite photocatalyst.

2. Material and methods

2.1. Material

All chemicals in this study were of analytical grade without any further purification. Melamine (AR, CH_4N_2O), P25 (AR, TiO_2), and ethanol (AR, C_2H_5OH) were purchased from Sinopharm Chemical Reagent Co., Ltd., (Beijing, China). 2,4-D was purchased from Shanghai Zhanyun Chemical Co., Ltd., (Shanghai, China).

2.2. Preparation of catalysts

P25/g-C_3N_4 photocatalyst were prepared by one-step roasting method. Firstly, P25 and melamine were ground and mixed thoroughly. Then, the mixtures were placed in covered ceramic crucible and calcinated at 550°C for 4 h in a muffle furnace. After cooling down to room temperature, the bright yellow product was successfully prepared. In the experiment, when the mass ratio of the raw material P25 and melamine was 1:100, 3:100, and 5:100, the final product obtained was 1 wt.%-P25/g-C_3N_4, 3 wt.%-P25/g-C_3N_4, and 5 wt.%-P25/g-C_3N_4 respectively, which can be labeled as 1%-P/CN, 3%-P/CN, and 5%-P/CN. As comparison, materials melamine and calcined P25 were also processed in the same routine to obtain g-C_3N_4 and P25 calcined, respectively. The as-prepared P25 calcine sample was labeled as "PC".

2.3. Characterization

Powder X-ray diffraction (XRD) patterns of samples were obtained using by Bruker D8 advance diffractometer (Germany) with Cu-Kα radiation (λ = 0.15418 nm). Fourier transform infrared spectroscopy (FT-IR) was measurement on affinity-1 FT-IR spectrometer using conventional KBr pellets in the range of 4,000–500 cm^{-1}. The UV-vis diffuse reflectance spectra (DRS) were characterized by Shimadzu UV2550 UV-visible spectrophotometer (Japan) with $BaSO_4$ as a reference. The scanning electron microscopy (SEM) images were observed by Hitachi S-4800 cold field emission scanning electron microscopy (Japan). The UV-vis DRS were characterized by Shimadzu UV2550 UV-visible spectrophotometer (Japan) with $BaSO_4$ as a reference. Photoluminescence (PL) study was recorded on fluorolog-TCSPC luminescence spectrometer. Electrochemical analysis was conducted on a CHI 760C workstation. The transient photocurrent responses analysis was conducted in 0.5 M Na_2SO_4 electrolyte under 300 W Xe lamp irradiation. Electrochemical impedance spectroscopy (EIS) was recorded by using an alternating voltage of 5 mV amplitude in the frequency range of 10^5 to 10^{-2} Hz with the open-circuit voltage in 0.5 M Na_2SO_4.

2.4. Evaluation of photocatalytic activity

The catalytic performance of the P25/g-C_3N_4 was tested by the photocatalytic ozonation experiment of 2,4-D. During the experiment, 0.05 g as-prepared catalyst was added into 100 mL 10 mg/L 2,4-D solution. Then, the suspension was stirred in the dark for 30 min to reach 2,4-D adsorption–desorption equilibrium. After that, the suspension was irradiated by a 300 W xenon lamp (λ > 420 nm), and ozone was introduced into suspension at a flow rate of 30 mL/min and a concentration of 14.2 mg/L. The suspension of calcined-P25 and P25/g-C_3N_4 would be sampled at intervals of 5 min while that of P25 was sampled at intervals of 10 min. Finally, the supernatant was collected by centrifugation and the concentration of 2,4-D of the supernatant was measured using an UV-2450 UV-vis spectrophotometer at λ_{max} = 283 nm. The degradation rate was calculated by the following formula:

$$\text{Degradation}\,(\%) = \left[\left(\frac{1-A_i}{A_0}\right)\right] \times 100\%. \quad (1)$$

where A_0 is the absorbance of the solution when the 2,4-D first reached the adsorption-desorption equilibrium, A_i is the absorbance of the solution after reacting for x minutes.

2.5. Active radicals capture experiments

The active radicals capture experiment was conducted to investigate the photocatalytic mechanism of 2,4-D degradation. In order to capture the generated hydroxyl radicals ($^{\bullet}OH$), holes (h^+), and $^{\bullet}O_3^-$, 1 mmol *tert*-butyl alcohol (TBA), ethylenediaminetetraacetic acid disodium (EDTA-2Na), and trichloromethane ($CHCl_3$) was added into the catalyst suspension in the catalyst photocatalytic ozonation experiments, respectively.

3. Results and discussion

3.1. XRD and FI-IR

The crystallographic structures of the obtained samples were analyzed by XRD and the results are shown in Fig. 1. It can be seen that pure g-C_3N_4 sample display two characteristic diffraction peaks at 13.1° and 27.4°, corresponding to its (100) and (002) crystal faces, respectively, indicating that the in-plane structural packing motif and the inter-planar stacking of aromatic system [19]. For the pure P25 samples, a series of characteristic diffraction peaks located at 25.7°, 38.4°, 48.6°, 54.4°, 55.4°, and 63.2°, which corresponds to its (101), (004), (200), (105), (211), and (204) faces, respectively [26]. After calcining, the crystal form of P25 Calcined did not change. In the case of the composite photocatalysts P25/g-C_3N_4, the characteristic diffraction peaks of g-C_3N_4 and P25 are well coexist in the patterns. Moreover, the intensity of the g-C_3N_4 diffraction peak is weakened as its proportion in the heterojunction P25/g-C_3N_4 decreases, while the diffraction peak of P25 is strengthened. The good crystallinity and purity of the composites implied that the P25/g-C_3N_4 heterostructure had been synthesized successfully. Furthermore, the coexist of the main characteristic peaks of P25 and /g-C_3N_4 means the successful combination between P25 and g-C_3N_4. To explore the surface functional groups and the interaction between P25 and g-C_3N_4, the FT-IR spectra of g-C_3N_4, P25 and 3%-P/CN are displayed in Fig. 2. There are a series of peaks at 1,464; 1,381; and 1,253 cm^{-1} in the composite photocatalyst, which are assigned to the stretching vibration of C–N and C=N [29]. The peak located at 1,627 and 472 cm^{-1} is ascribed to the C=N stretching vibration and the typical stretching vibration of Ti–O–Ti, respectively [30]. The above analysis demonstrates that catalysts P25/g-C_3N_4 were well prepared. Notably, the spectrum of 3%-P/CN samples includes the characteristic peaks of P25 and g-C_3N_4, which further means that the successful formation of composite photocatalyst.

3.2. SEM and TEM

To investigate the morphology of the synthesized samples, the SEM image of the P25, g-C_3N_4 and 3%-P/CN were obtained in Fig. 3. In Fig. 3a, the P25 is composed of nanoparticles with an average size of about 25 nm and shows an agglomerated morphology. The image in Fig. 3b exhibited the SEM of P25 Calcined was no different from P25. As shown in Fig. 3c, g-C_3N_4 was composed of bulks and had a typical laminated structure with obvious agglomeration. In Fig. 3d, after the introduction of P25, the P25 nanoparticles were evenly supported on the surface of g-C_3N_4.

To further explore the structure and morphology of P25/g-C_3N_4, TEM, and HR-TEM were employed and shown in Fig. 4. From the chart, we can see that P25 nanoparticles with an average particle size of about 25 nm were evenly supported on the surface of layered g-C_3N_4. Furthermore, the HRTEM image in Fig. 4b displays the interplanar spacings of P25 are 0.35 and 0.29 nm, corresponding to the (101) planes of anatase TiO_2 and (110) planes of rutile TiO_2, respectively. The results show the combination of the two lattices of P25 and g-C_3N_4 in 3%P-CN samples [31].

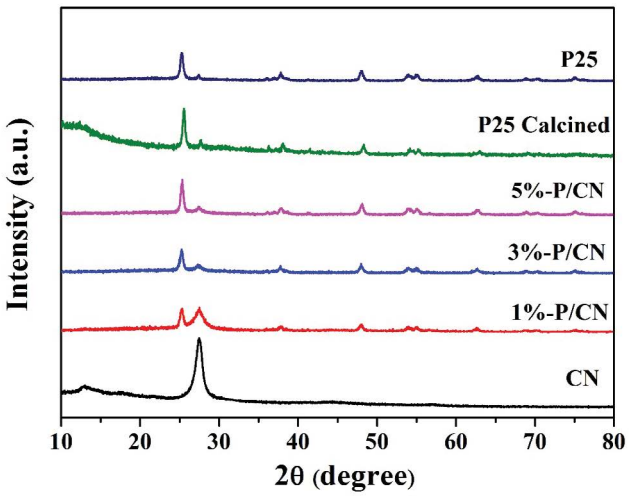

Fig. 1. XRD patterns of the as-synthesized samples.

3.3. UV-vis and PL

To explore the optical absorption properties, Fig. 5 demonstrates the UV-vis absorption spectrum of as-synthesized samples. It displayed that pure g-C_3N_4 exhibit photoresponse in the visible region with an absorption sideband about 480 nm, while P25 was only in the ultraviolet region. As a result, the P25/g-C_3N_4 composite showed a gradual blue shift of absorption sideband with the increasing amount of P25. To study the charge separation and transfer efficiency of the obtained samples, the photoluminescence (PL) spectra were carried out at an excitation wavelength of 360 nm. As shown in Fig. 6, pure phase g-C_3N_4 and heterojunction 3%-P/CN both shown fluorescence emission peaks at the wavelength of 460 nm, and the emission peak intensity of g-C_3N_4 is significantly higher than that of 3%-P/CN, indicating that the incorporation of P25 could promote the photo-generated carrier separation efficiency [32].

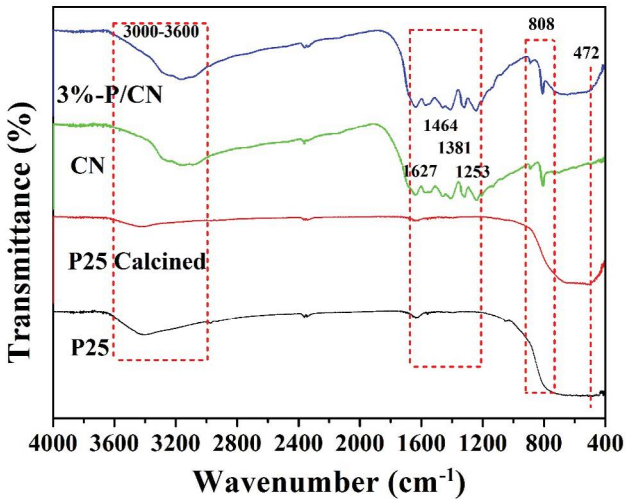

Fig. 2. FT-IR spectra of g-C_3N_4, P25, P25 calcined, and 3%-P/CN heterojunctions.

3.4. Catalytic performance

The photocatalytic ozonation activities of prepared composite photocatalyst were assessed by the degradation of 2,4-D under visible-light irradiation and the results are displayed in Fig. 7. It can be seen from Fig. 8b that P25/g-C_3N_4 catalysts showed poor photocatalytic degradation activity in the absence of ozone. However, P25 Calcined showed a higher photocatalytic activity with the degradation rate of 2,4-D reached 17.5% (vis/PC), which is much higher than that of P25. It is due to the fact calcination treatment enhanced the phase transformation of the P25 TiO_2 powders from amorphous to anatase. When ozone is introduced into the degradation system, as shown in Fig. 7a, the degradation ratio of 2,4-D was only 17.1% (Dark/O_3) for ozonation alone with the ozone concentration of 30 mL/min in 60 min. When P25/CN catalyst was added into ozonation system under visible-light irradiation, the degradation efficiency of 2,4-D was greatly improved. Among them, the 3%-P/CN catalyst (vis/3%-P/CN/O_3) showed the highest catalytic activity, and the 2,4-D degradation rate reached 90.2% in 30 min,

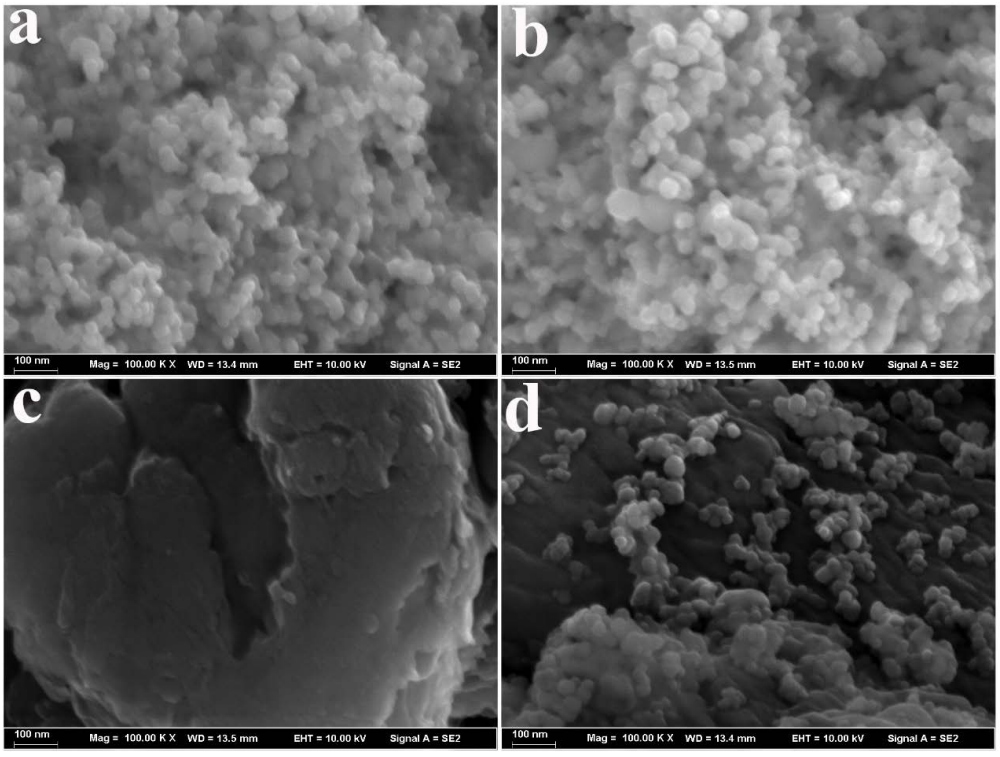

Fig. 3. SEM images of (a) P25, (b) P25 Calcined, (c) g-C_3N_4, and (d) EDS of 3%-P/CN.

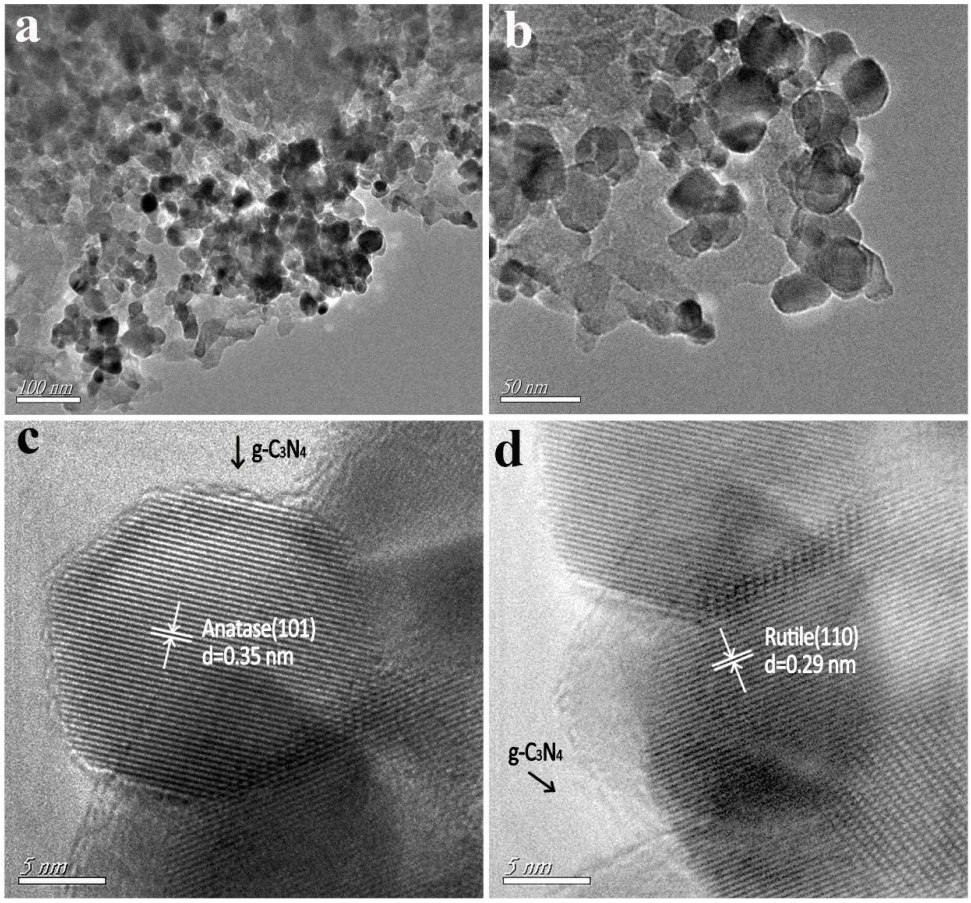

Fig. 4. TEM (a and b) and HRTEM (c and d) images of the 3%-P/CN sample.

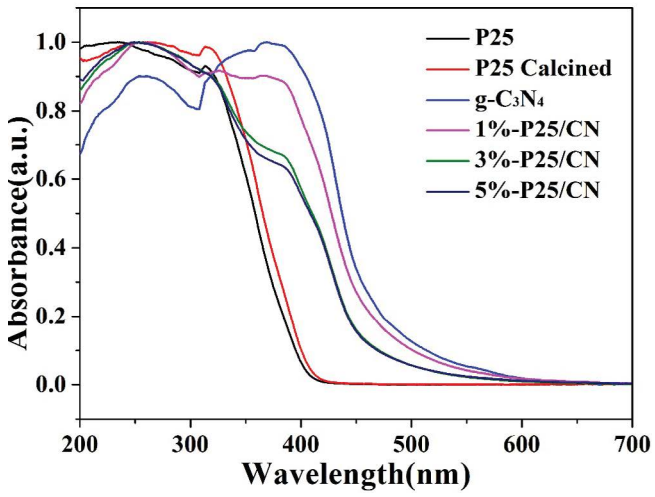

Fig. 5. UV-vis spectra of the as-synthesized samples.

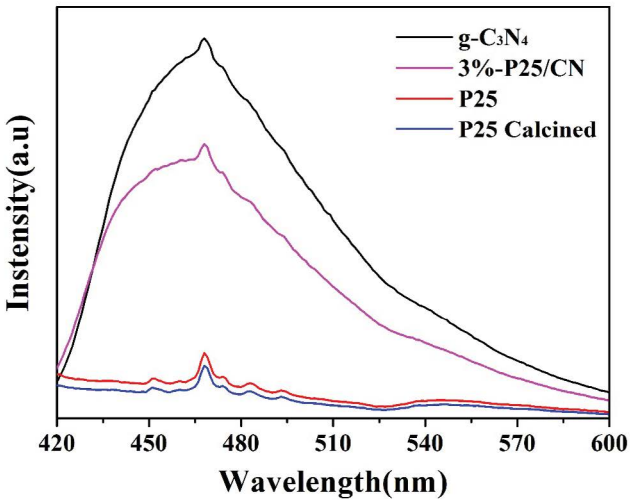

Fig. 6. PL spectra of g-C_3N_4, P25, P25 calcined, and 3%-P/CN samples at the excitation wavelength of 360 nm.

and degradation activity of catalysts 1%-P/CN (vis/1%-P/CN/O_3) and 5%-P/CN (vis/5%-P/CN/O_3) reached 86.3% and 62.4% in 30 min, respectively. The significant improvement in catalytic activity may be attributed to the synergy between ozone oxidation and photocatalytic oxidation.

Since the photocatalytic ozonation degradation process of 2,4-D can be regarded as a pseudo-first-order reaction, and the rate constants for vis/$^{\bullet}O_3$, vis/3%-P/CN, vis/3%-P/CN/$^{\bullet}O_3$ were turned out to be 0.0071, 0.0014, and 0.0794 1/

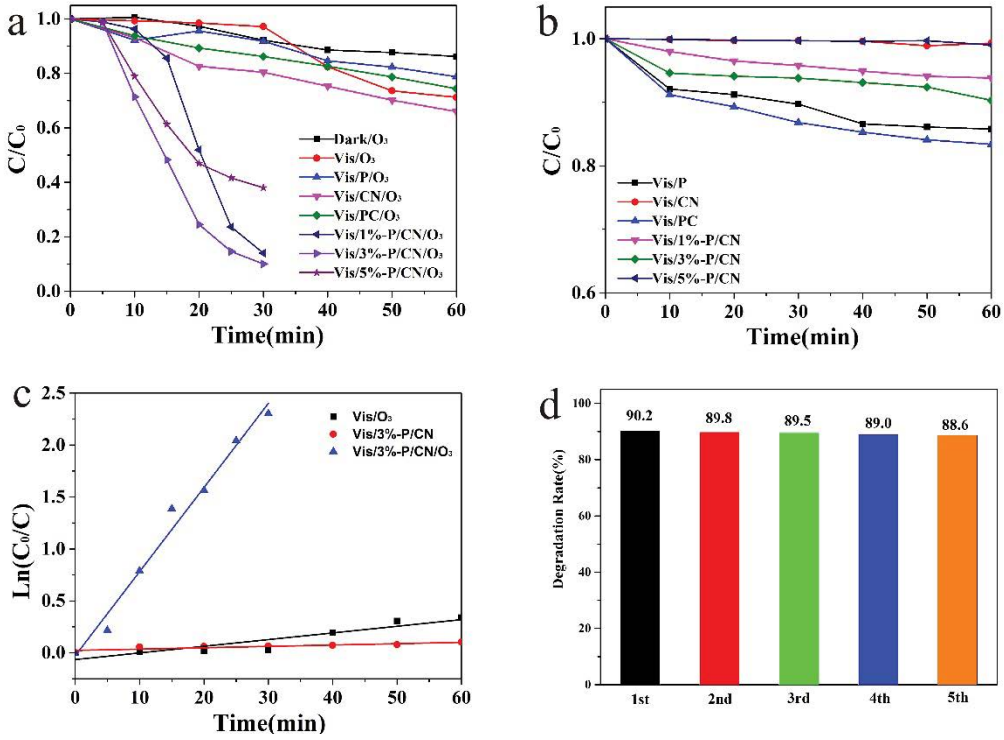

Fig. 7. (a) Photocatalytic ozonation and (b) photocatalytic degradation of 2,4-D over as-synthesized photocatalysts under visible-light irradiation; (c) the first-order-kinetic reaction for removal of 2,4-D by different processes and (d) cycling runs for the photocatalytic oxidation degradation of 2,4-D in the presence of 3%-P/CN sample.

min in Fig. 7c, respectively. Generally speaking, the synergy factor can be used to descript the synergistic effect in the photocatalytic ozonation of 2,4-D, and it can be calculated by the following formula [8]:

$$\text{Synergistic Factor}(\text{SF}) = \frac{K_{app}\ \text{photocatalytic ozonation}}{K_{app}\ \text{ozonation} + K_{app}\ \text{photocatalysis}} = \frac{0.0794}{0.0071 + 0.0014} = 9.34 > 1 \quad (2)$$

The synergistic factor is 9.34, indicates that there is a stronger synergy between photocatalytic oxidation and ozone oxidation during the reaction. Fig. 7d shows five cycling experiments of 3%-P/CN for 2,4-D photocatalytic ozonation. It can be clearly observed that after five times reuse, the activity of the catalyst hardly changed, which indicated that the prepared P25/g-C_3N_4 composite photocatalyst has strong stability under the experiment condition.

3.5. Photocurrent response and EIS

The transient photocurrent responses and EIS were used to testify the separation and transfer efficiency of photo-generated carrier, and the results are recorded in Fig. 8. It can be seen from Fig. 8a that the photocurrent density obtained with 3%-P/CN is higher than that of the pure g-C_3N_4 and P25, which implies that 3%-P/CN composite has higher photogenerated charge mobility. Fig. 8b compares the EIS plot of P25/g-C_3N_4, g-C_3N_4, and P25, and the arc diameter in the EIS plot of P25/g-C_3N_4 is smaller than that of other samples under the same conditions. Generally speaking, the smaller arc diameter indicates a lower resistance of the interfacial charge transfer, which further proves that the 3%-P/CN composite has more effective charge separation and transfer efficiency.

3.6. Active species capturing experiment

In order to investigate the main reactive species in the photocatalytic degradation of 2,4-D over P25/g-C_3N_4 composite photocatalysts, a series of radical trapping experiments were performed. In the experiment, radical scavengers tBA, EDTA-2Na, and $CHCl_3$ were used to quench $^{\bullet}OH$, h^+, and e^-, respectively [33]. As depicted in Fig. 9, when tBA and $CHCl_3$ were added, the degradation rates of 2,4-D decreased apparently from 90.2% to 40.3% and 22.7%, respectively. And when EDTA-2Nawas added, the catalytic degradation of 2,4-D is only slightly affected. The results indicate that active specie $^{\bullet}O_3^-$ and $^{\bullet}OH$ play major roles in this degradation reaction. When adding N_2 without O_3, the degradation rate dropped from 89% to less than 2%, indicating that O_3 plays an important role in photocatalytic ozonation under visible light irradiation.

3.7. Photocatalytic ozonation mechanism

Based on the above analysis, we proposed a possible mechanism for the photocatalytic ozonation degradation of 2,4-D by P25/g-C_3N_4 heterojunction under visible light

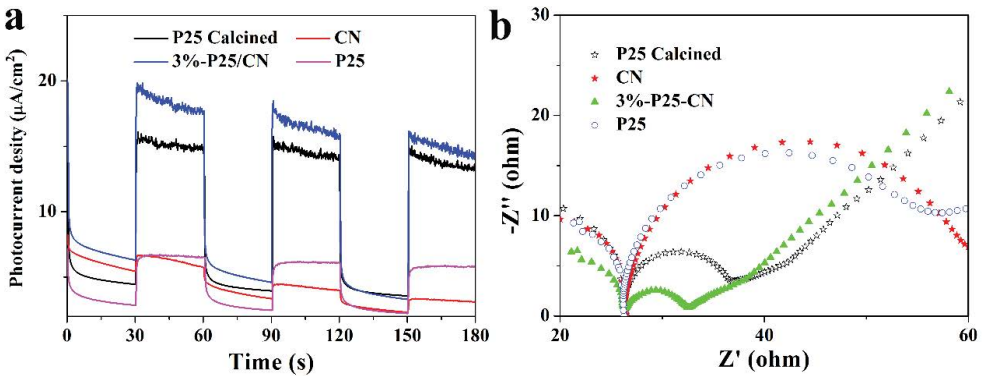

Fig. 8. (a) Photocurrent responses and (b) EIS Nyquist plot of as-synthesized photocatalysts.

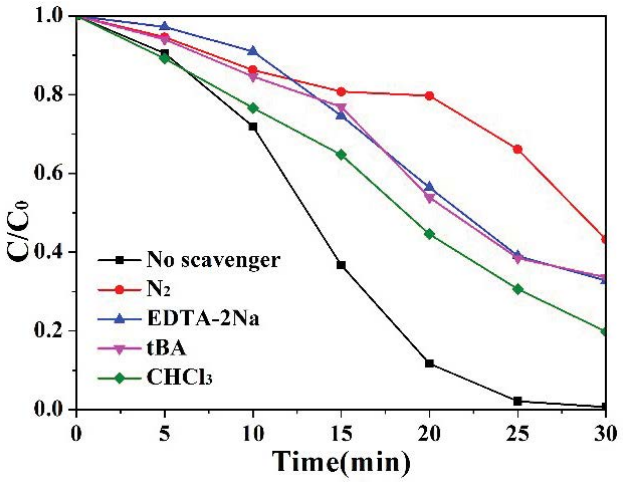

Fig. 9. Trapping experiments of active species during the photocatalytic ozonation degradation of 2,4-D over 3%-P/CN photocatalyst under visible light irradiation.

irradiation and the result is illustrated in Fig. 10. Firstly, g-C_3N_4 could be easily excited under visible light, electrons and holes would form on the CB and VB of g-C_3N_4, respectively. However, it is hard for P25 nanoparticles to generate holes and electrons because of the broader bandgap. Then, the photo-generated electrons on the CB of g-C_3N_4 would transferred to the CB of P25, and the photo-generated holes on the VB of P25 would transferred to the VB of g-C_3N_4, which can effectively promote the transfer of photo-generated charges. After that, the injected-electrons would be trapped by ozone to give $^{\bullet}O_3^-$, which would immediately react with H^+ in solution to produce $^{\bullet}HO_3$ for the formation of reactive species $^{\bullet}OH$ to degrade 2,4-D. In addition, ozone would be decomposed into active oxygen atoms and oxygen by the irradiation of ultraviolet light, in which the active oxygen atoms can react with water to generate $^{\bullet}OH$ to degrade 2,4-D. In the meanwhile, the holes accumulated on the VB of g-C_3N_4 can directly degrade 2,4-D.

The process was described as follows:

$$O_3 + e^- \rightarrow {}^{\bullet}O_3^- \quad (3)$$

$$^{\bullet}O_3^- + H^+ \rightarrow {}^{\bullet}HO_3 \quad (4)$$

$$^{\bullet}HO_3 \rightarrow {}^{\bullet}OH + O_2 \quad (5)$$

$$O_3 \rightarrow O_2 + O \quad (6)$$

$$O + H_2O \rightarrow H_2O_2 \rightarrow 2{}^{\bullet}OH \quad (7)$$

$$h^+ / {}^{\bullet}OH / O + 2,4\text{-D} \rightarrow \text{Degradation products} \quad (8)$$

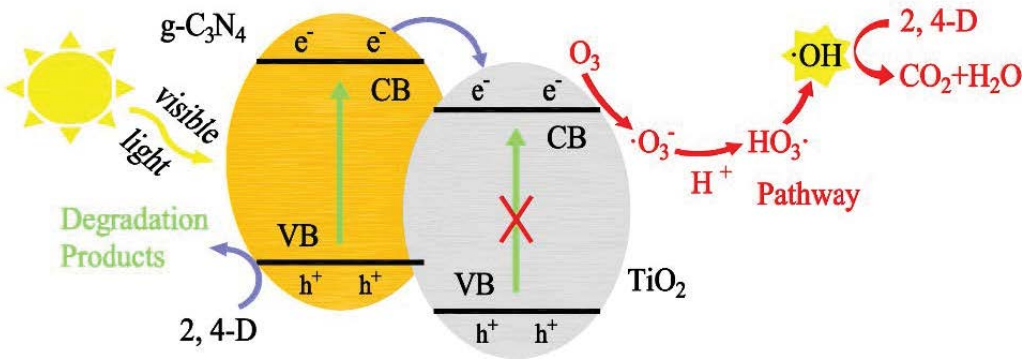

Fig. 10. Proposed mechanism of photocatalytic ozonation of 2,4-D for P25/g-C_3N_4.

4. Conclusion

In general, a series of the different mass ratio of P25/g-C_3N_4 are produced by one-step method, and all the as-prepared composites shows excellent photocatalytic ozonation performance for degrading 2,4-D under visible light irradiation. 3%-P/CN shows the best photocatalytic ozonation activity for the degradation of 2,4-D (90.2%) in 30 min. The promoted photocatalytic ozonation capability was attributed to efficient separation of the electron-hole pairs resulting from P25/g-C_3N_4 heterojunction, which verified by the lowest PL respond and the best photocurrent response and EIS results. Besides, the trapping experiment displayed that $^{\bullet}O_3^-$ and $^{\bullet}OH$ were the main active species and the synergistic effects between ozonation and photocatalysis attributed to the powerful scavenger effect of ozone and strong activity of $^{\bullet}OH$ radicals. Furthermore, the repetitive experiment illustrates that 3%-P/CN has strong stability. The above results indicate that P25/g-C_3N_4 is a potential catalyst that will be of great importance for water purification.

Acknowledgments

This work is supported by the National Natural Science Foundation of China (21906039, 21906072), Natural Science Foundation of Shaanxi Province (2019JQ-382), Funding project for introduced overseas scholars of Hebei Province (C20190321), Fundamental Research Funds for the Central Universities of Chang'an University (300102290501), Program for water resources research and promotion of Hebei Province (2019–55), and Doctoral research fund of Hebei Geo University (BQ2019041).

References

[1] F. Islam, J. Wang, M.A. Farooq, M.S. Khan, L. Xu, J. Zhu, M. Zhao, S. Muños, Q. Li, W. Zhou, Potential impact of the herbicide 2,4-dichlorophenoxyacetic acid on human and ecosystems, Environ. Int., 111 (2018) 332–351.

[2] Y.H. Zhou, P.Y. Li, M.J. Chen, Z.H. Dong, C.Y. Lu, Groundwater quality for potable and irrigation uses and associated health risk in southern part of Gu'an County, North China Plain, Environ. Geochem. Health, (2020), https://link.springer.com/article/10.1007/s10653-020-00553-y.

[3] M. Golshan, B. Kakavandi, M. Ahmadi, M. Azizi, 2018 Photocatalytic activation of peroxymonosulfate by TiO_2 anchored on cupper ferrite (TiO_2@$CuFe_2O_4$) into 2, 4-D degradation: process feasibility, mechanism and pathway, J. Hazard. Mater., 359 (2018) 325–337.

[4] G.D. Okcua, H.E. Oktenb, A. Yalcuk, Heterogeneous photocatalytic degradation and mineralization of 2,4-dichlorophenoxy acetic acid (2,4-D): its performance, kinetics, and economic analysis, Desal. Water Treat., 137 (2019) 312–327.

[5] W.L. Shi, M.Y. Li, X.L. Huang, H.J. Ren, F. Guo, Y.B. Tang, C.Y. Lu, Construction of $CuBi_2O_4/Bi_2MoO_6$ *p-n* heterojunction with nanosheets-on-microrods structure for improved photocatalytic activity towards broad-spectrum antibiotics degradation, Chem. Eng. J., 394 (2020) 125009–125018.

[6] F. Guo, X.L. Huang, Z.H. Chen, H.J. Ren, M.Y. Li, L.Z. Chen, MoS_2 nanosheets anchored on porous $ZnSnO_3$ cubes as an efficient visiblelight-driven composite photocatalyst for the degradation of tetracycline andmechanism insight, J. Hazard. Mater., 390 (2020) 122158–122169.

[7] L. Sánchez, J. Peral, X. Domènech, Aniline degradation by combined photocatalysis and ozonation, Appl. Catal., B, 19 (1998) 59–65.

[8] W. Zhao, Y. Liu, Z. Wei, S. Yang, H. He, C. Sun, Fabrication of a novel *p-n* heterojunction photocatalyst *n*-$BiVO_4$@*p*-MoS_2 with core–shell structure and its excellent visible-light photocatalytic reduction and oxidation activities, Appl. Catal., B, 185 (2016) 242–252.

[9] M.H. Dehghani, Y. Karamitabar, F. Changani, Z. Heidarinejad, High performance degradation of phenol from aqueous media using ozonation process and zinc oxide nanoparticles as a semiconductor photo catalyst in the presence of ultraviolet radiation, Desal. Water Treat., 166 (2019) 105–114.

[10] D.H. Quinones-Murillo, A.A. Ariza-Reyes, L.J. Ardila-Velez, Some kinetic and synergistic considerations on the oxidation of the azo-compound Ponceau 4R by solar-mediated heterogeneous photocatalytic ozonation, Desal. Water Treat., 170 (2019) 61–74.

[11] J.L. Li, W.S. Guan, X. Yan, Z. Wu, W.D. Shi, Photocatalytic ozonation of 2,4-dichlorophenoxyacetic acid using $LaFeO_3$ photocatalyst under visible light irradiation, Catal. Lett., 148 (2018) 23–29.

[12] M. Sheydaei, H.R.K. Shiadeh, B. Ayoubi-Feiz, R. Ezzati, Preparation of nano N-TiO_2/graphene oxide/titan grid sheets for visible light assisted photocatalytic ozonation of cefixime, Chem. Eng. J., 353 (2018) 138–146.

[13] W.L. Shi, M.Y. Li, X.L. Huang, H.J. Ren, C. Yan, F. Guo, Facile synthesis of 2D/2D $Co_3(PO_4)_2$/g-C_3N_4 heterojunction for highly photocatalytic overall water splitting under visible light, Chem. Eng. J., 382 (2019) 122960–122968.

[14] X.F. Chen, J.S. Zhang, X.Z. Fu, M. Antonietti, X.C. Wang, Fe-g-C_3N_4-catalyzed oxidation of benzene to phenol using hydrogen peroxide and visible light, J. Am. Chem. Soc., 131 (2009) 11658–11659.

[15] J.F. Guo, P.T. Li, Z. Yang, A novel Z-scheme g-$C_3N_4/LaCoO_3$ heterojunction with enhanced photocatalytic activity in degradation of tetracycline hydrochloride, Catal. Commun., 122 (2019) 63–67.

[16] N. Tian, H. Huang, Y. Guo, Y. He, Y. Zhang, A g-$C_3N_4/Bi_2O_2CO_3$ composite with high visible-light-driven photocatalytic activity for rhodamine B degradation, Appl. Surf. Sci., 322 (2014) 249–254.

[17] F. Guo, M.Y. Li, H.J. Ren, X.L. Huang, K.K. Shu, W.L. Shi, C.Y. Lu, Facile bottom-up preparation of Cl-doped porous g-C_3N_4 nanosheets for enhanced photocatalytic degradation of tetracycline under visible light, Sep. Purif. Technol., 228 (2019) 115770–115776.

[18] F. Guo, L.J. Wang, H.R. Sun, M.Y. Li, W.L. Shi, High-efficiency photocatalytic water splitting by a N-doped porous g-C_3N_4 nanosheet polymer photocatalyst derived from urea and N,N-dimethylformamide, Chem. Front., 7 (2020) 1770–1779.

[19] K.Z. Qi, S.Y. Liu, R. Selvaraj, W. Wang, Z.X. Yan, Comparison of Pt and Ag as co-catalyst on g-C_3N_4 for improving photocatalytic activity: experimental and DFT studies, Desal. Water Treat., 153 (2019) 244–252.

[20] Y. Li, S. Wu, L. Huang, H. Xu, R. Zhang, M. Qu, Q. Gao, H. Li, g-C_3N_4 modified Bi_2O_3 composites with enhanced visible-light photocatalytic activity, J. Phys. Chem. Solids, 76 (2015) 112–119.

[21] F. Guo, X.L. Huang, Z.H. Chen, H.R. Sun, L.Z. Chen. Prominent co-catalytic effect of CoP nanoparticles anchored on highcrystalline g-C_3N_4 nanosheets for enhanced visible-light photocatalytic degradation of tetracycline in wastewater, Chem. Eng. J., 395 (2020) 125118–125120.

[22] T. Xiao, Z. Tang, Y. Yang, L. Tang, Y. Zhou, Z. Zou, *In situ* construction of hierarchical WO_3/g-C_3N_4 composite hollow microspheres as a Z-scheme photocatalyst for the degradation of antibiotics, Appl. Catal., B, 220 (2018) 417–428.

[23] F. Guo, H.R. Sun, X.L. Huang, W.L. Shi, C. Yan, Fabrication of TiO_2/high-crystalline g-C_3N_4 composite with enhanced visible-light photocatalytic performance for tetracycline degradation, J. Chem. Technol. Biotechnol., 95 (2020) 2684–2693.

[24] X.Z. Yue, S.S. Yi, R.W. Wang, Z.T. Zhang, S.L. Qiu, Well-controlled $SrTiO_3$@Mo_2C core-shell nanofiber photocatalyst: boosted photo-generated charge carriers transportation and enhanced catalytic performance for water reduction, Nano Energy, 47 (2018) 463–473.

[25] F. Tavakoli, A. Badiei, M.S. Niasari, Efficient photodegradation of acid orange 7 by using ultrasound-assisted synthesis of

ternary graphene nanocomposite based on TiO_2, Desal. Water Treat., 147 (2019) 334–342.
[26] Y. Sheng, Z. Wei, H. Miao, W. Yao, H. Li, Y. Zhu, Enhanced organic pollutant photodegradation via adsorption/photocatalysis synergy using a 3D g-C_3N_4/TiO_2 free-separation photocatalyst, Chem. Eng. J., 370 (2019) 287–294.
[27] Y. Tan, Z. Shu, J. Zhou, T. Li, W. Wang, Z. Zhao, One-step synthesis of nanostructured g-C_3N_4/TiO_2 composite for highly enhanced visible-light photocatalytic H_2 evolution, Appl. Catal., B, 230 (2018) 260–268.
[28] S. Zhou, Y. Liu, J. Li, Y. Wang, G. Jiang, Z. Zhao, D. Wang, A. Duan, J. Liu, Y. Wei, Facile in situ synthesis of graphitic carbon nitride (g-C_3N_4)-N-TiO_2 heterojunction as an efficient photocatalyst for the selective photoreduction of CO_2 to CO, Appl. Catal., B, 158–159 (2014) 20–29.
[29] D. Zeng, W.J. Ong, Y. Chen, S.Y. Tee, C.S. Chua, D.L. Peng, M.Y. Han, Co_2P nanorods as an efficient cocatalyst decorated porous g-C_3N_4 nanosheets for photocatalytic hydrogen production under visible light irradiation, Part. Part. Syst. Char., 35 (2018) 1700251–1700257, doi: 10.1002/ppsc.201700251.
[30] J. Wang, J. Huang, H. Xie, A. Qu, Synthesis of g-C_3N_4/TiO_2 with enhanced photocatalytic activity for H_2 evolution by a simple method, Int. J. Hydrogen Energy, 39 (2014) 6354–6363.
[31] C.Y. Lu, F. Guo, Q.Z. Yan, Z.J. Zhang, D. Li, L.P. Wang, Y.H. Zhou, Hydrothermal synthesis of type II $ZnIn_2S_4$/$BiPO_4$ heterojunction photocatalyst with dandelion-like microflower structure for enhanced photocatalytic degradation of tetracycline under simulated solar light, J. Alloys Compd., 811 (2019) 151976–151985, doi: 10.1016/j.jallcom.2019.151976.
[32] L.P. Wang, T.T. Huang, G.P. Yang, C.Y. Lu, F.L. Dong, Y.L. Li, W.S. Guan, The precursor-guided hydrothermal synthesis of $CuBi_2O_4$/WO_3 heterostructure with enhanced photoactivity under simulated solar light irradiation and mechanism insight, J. Hazard. Mater., 381 (2020) 120956–120967.
[33] L.P. Wang, G.P. Yang, D. Wang, C.Y. Lu, W.S. Guan, Y.L. Li, J. Deng, J. Crittenden, Fabrication of the flower-flake-like $CuBi_2O_4$/Bi_2WO_6 heterostructure as efficient visible-light driven photocatalysts: performance, kinetics and mechanism insight, Appl. Surf. Sci., 495 (2019) 143521–143533, doi: 10.1016/j.apsusc.2019.07.263.